- Technical Paper -

PREDICTION OF CORROSION-INDUCED CRACK WIDTH DISTRIBUTION: COMPARING 3D FE AND EXPERIMENTAL RESULTS

Mingyang ZHANG[*1], Mina SHINTANI[*2], Jiyu XIN[*3] and Mitsuyoshi AKIYAMA[*4]

ABSTRACT

In this study, non-uniform steel corrosion along the corroded rebar and the associated longitudinal crack width of RC beams at various corrosion levels were monitored by X-ray and digital image processing techniques. A three-dimensional (3D) finite element (FE) model was established based on a half ellipses-shape corrosion expansion model to simulate the corrosion-induced crack width distribution. A comparison between numerical and experimental results was conducted. The 3D FE model provided a good agreement with experimental distribution of corrosion crack width.

Keywords: non-uniform corrosion, crack width, finite element method, X-ray, image processing

1. INTRODUCTION

Corrosion-induced cracking is a major cause of deterioration in reinforced concrete (RC) structures in chloride-containing environments. The highly alkaline nature of concrete prevents the corrosion of reinforcing bars by a passive film. However, the corrosion can occur when the passive film partly or completely breaks down due to the chloride ion attack. The volumetric expansion of corrosion products leads to cracking of cover concrete. Consequently, the aggressive agents can easily reach to the rebar surface to accelerate the corrosion process. The corrosion of reinforcing bars can lead to serviceability failure and deterioration of long-term structural performance. Therefore, there is a well-justified need for a thorough investigation of the cracking process and crack width of concrete, as crack width is a common visual indicator to evaluate the deterioration level of in situ corroded RC structures [1].

A number of empirical and analytical models and numerical techniques for describing the cracking process of concrete induced by steel corrosion have been proposed [2−4]. Based on a comparison of surface crack width propagation between model-computed and experimental results, none of the empirical models provides a good prediction for all of the experimental data, since the empirical model cannot consider all of the influencing parameters [5]. On the other hand, the analytical model has assumed that material corrosion is uniform over the structures. However, the penetration of chloride, moisture, and oxygen into concrete is often not uniform. More corrosion products are usually found on the side of the rebar that faces the concrete surface [6]. Lim et al. [7] and Zhang et al. [8] carried out the accelerated corrosion test on RC specimens and applied X-ray and image processing techniques to monitor the spatial variability of steel corrosion and obtain corrosion-induced crack width distribution along the longitudinal rebar of RC beams. Their experimental results demonstrated that the distributions of steel corrosion and crack width are spatially non-uniform.

Apart from the experimental efforts, numerous studies have been performed by using the nonlinear finite element (FE) method [9, 10]. Zhao [11] pointed out that FE analysis is an efficient way to study the corrosion-induced concrete cracking with the real distribution of corrosion around the rebar circumference. The non-uniform corrosion expansion is treated as prescribed displacement applied to the concrete cover. The vast majority of numerical models have been proposed for modeling concrete cracks induced by corrosion products based on the two-dimensional (2D) FE model ignoring the spatial distribution along the rebar. To address this problem, a three-dimensional (3D) FE model has to be considered. Although the commercial software packages have made it easier to perform 3D FE analysis, further research is needed to predict the corrosion-induced crack width considering the spatial distribution over the RC beams.

In this paper, the non-uniform steel corrosion along the corroded rebar and the associated longitudinal crack width of RC beams at various corrosion levels were monitored by X-ray and digital image processing techniques. A 3D FE model is proposed based on a half ellipses-shape corrosion expansion model to simulate the crack development along the longitudinal direction of the beam. The distributions from experimental crack width were compared with those from the 3D FE model.

2. EXPERIMENTAL CONTEXT

2.1 Specimen Details

*1 Graduate School of Creative Science and Engineering, Waseda University, JCI Student Member
*2 Graduate School of Creative Science and Engineering, Waseda University
*3 Graduate School of Creative Science and Engineering, Waseda University
*4 Prof., Dept. of Civil and Environmental Engineering, Waseda University, Dr.E., JCI Member

Three specimens with a size of 1460 × 80 × 140 mm were cast with a cover of 20 mm. Table 1 and Fig. 1 show the details of test specimens. Each specimen was reinforced with one deformed steel bar with a diameter of 13 mm (i.e., DB13). Different current densities of 50, 100, and 200 μA/cm^2 were applied to accelerate the corrosion of longitudinal rebar. Table 2 shows the mixing proportions of concrete. The coarse aggregate has a specific density of 2640 kg/m^3 and a maximum size of 20 mm. Fine aggregate has a fineness modulus of 2.64 and a specific density of 2600 kg/m^3. 6-mm-diameter rebar was used as stirrups.

Table 1 Specimens details

Specimen	Cross-section (mm)	Current density (I_{corr}) (μA/mm^2)	Concrete compressive strength (MPa)
SP1	140 × 80	50	34.9
SP2	140 × 80	100	34.9
SP3	140 × 80	200	34.9

Table 2 Mixing proportions

Water (kg/m^3)	Cement (kg/m^3)	FA[a] (kg/m^3)	CA[b] (kg/m^3)	AE[c] (kg/m^3)
181	362	754	961	2715

[a] Fine aggregate; [b] Coarse aggregate; and [c] Air entrained water-reducing agent

2.2 Accelerated Corrosion Test

After curing of concrete for 28 days, the specimens were subjected to accelerated corrosion using the impressed current method. Fig. 2 shows the accelerated corrosion test setup. The RC specimens were partially immersed in a 3.0% NaCl solution. The accelerated corrosion process was achieved by applying a constant current to the longitudinal rebar by a power supply. The steel bar acts as an anode, and the copper net submerged in the NaCl solution acts as a cathode. In order to move the specimens out of the tank to perform the measurement of crack width and X-ray radiography, the corrosion process was started and halted at three corrosion levels of approximately 2.5%, 7%, and 12%.

2.3 Measurement of Steel Weight Loss by X-Ray Photography

The spatial distribution of steel weight loss of rebar embedded in the beams at different corrosion levels was monitored and quantified using X-ray and digital image processing techniques. Fig. 3 shows the X-ray imaging setup. During the corrosion process, the images of original and corroded rebars in beams were acquired by X-ray apparatus from 8 viewing angles. Steel weight loss (Rw) per 5-mm along the longitudinal rebar was estimated using image processing technique. More detailed descriptions are provided in Zhang et al. [8]. Rw can be calculated as follows:

$$Rw = \frac{1}{k}\sum_{n=1}^{8}\frac{W_{\theta n} - W'_{\theta n}}{W_{\theta n}} \quad (1)$$

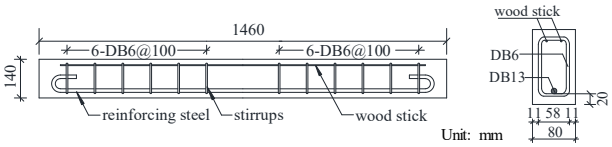

Fig. 1 Front view and cross-section of RC specimens

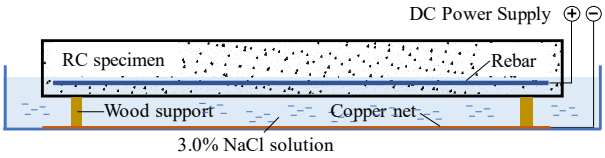

Fig. 2 Accelerated corrosion test setup

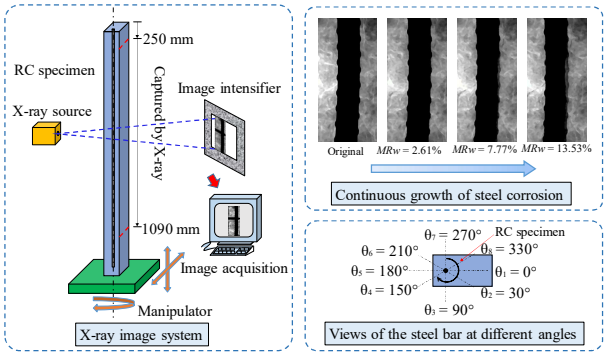

Fig. 3 X-ray imaging setup

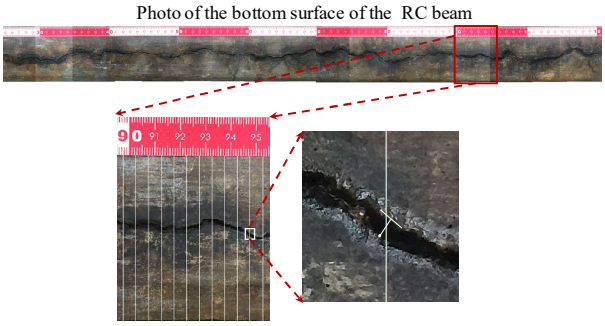

Fig. 4 Measurement of crack width

where $W_{\theta n}$ and $W'_{\theta n}$ are the weights of original and corroded rebars at 5-mm length with the n-th viewing angle θn, respectively; and k = 8 is the number of viewing angles. It should be noted that the mean steel weight loss (MRw) of the corroded rebar was calculated using all Rw measured at 5-mm length. The results of the distribution of Rw refer to the mean value of every 10-mm length along the rebar, which will also be used as the input in the FE model.

2.4 Corrosion Crack Width Measurement

The longitudinal crack that occurred along the bottom of the beam was measured at various stages of corrosion, as shown in Fig. 4. The procedure to measure the crack width involves the following steps. A millimeter-scale measuring tape was pasted on the surface close to the crack. The camera was placed on the top of a wood plank to maintain a constant distance to the surface while it was moved along the crack line for

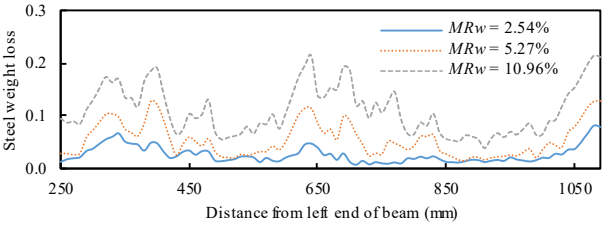

(a)

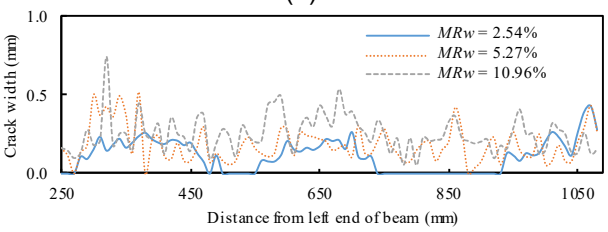

(b)

Fig. 5 Distribution of (a) steel weight loss, and (b) corresponding crack width at various corrosion levels of beam SP1

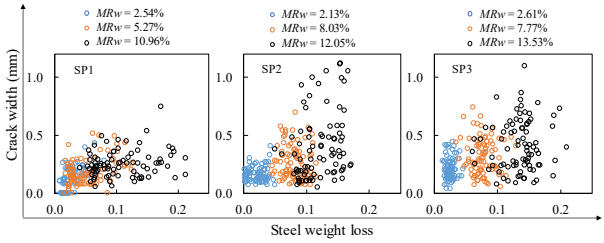

Fig. 6 Relationship between the crack width and steel weight loss of all beams

taking photos from one location to another. After taking the crack photos, the measurement of crack width was carried out using Image-Pro Plus software. The crack width measurement in Image-Pro Plus is in pixel, which can be converted to real crack width by a modification ratio based on the real length of the measuring tape in the photo (i.e., 436-pixel distance in image processing software equals to 10 mm in real length). The crack width was measured every 5 mm along the beam length and the crack width was denoted as *Cw*.

2.5 Distribution of Steel Weight Loss and Crack Width

Fig. 5 shows the example of spatial variability associated with the steel weight loss and corrosion crack width of corroded RC beam SP1. It can be seen that the distribution of steel weight loss over the RC beam is spatially non-uniform. A single crack along the longitudinal rebar appeared on the bottom surface of the beam. It is found that the corrosion-induced crack width also distributes non-uniformly along the beam due to the non-uniform steel corrosion. Fig. 6 shows the relationship between steel weight loss and crack widths at their corresponding locations for all the beams. It is found that the crack width increases with the steel weight loss, and higher current density would lead to larger crack width. Since corrosion product produced by the low current density was formed at a much slower rate than that produced by the high current density, it might take a considerable time to fill the concrete pores structures surrounding the rebar before inducing the cover cracking. In addition, the dispersion degree of crack width at one given steel weight loss increases with the steel weight loss. The relationship between steel weight loss and crack width weakens significantly at higher steel weight loss. Therefore, it is difficult to use a linear model for the relationship between steel weight loss and crack width because of such high uncertainty [2].

3. FINITE ELEMENT MODELING FOR NON-UNIFORM CORROSION-INDUCED COVER CRACKING

3.1 3D FE Model and Basic Hypotheses

In this paper, a 3D non-linear FE analysis was conducted to simulate the corrosion-induced cracking using DIANA [12] – a commercial non-linear FE software package. The FE model of the RC beam is shown in Fig. 7. The concrete is modeled by using eight-node solid element. The displacement constraints are imposed on the top surface of the beam. The rebar is modeled as a "hole" in the FE model, and the non-uniform corrosion around the rebar perimeter and along the rebar are simulated by applying prescribed radial displacement to the "hole" representing steel corrosion expansion.

Due to the complexities of concrete cracking process induced by steel corrosion, the following assumptions are made:

(1) The non-uniform corrosion around the rebar perimeter induces a non-uniform radial expansive pressure on the surrounding concrete; a corrosion distribution curve with an elliptic expression was employed to describe the expansion behavior of rust at the cross-section of rebar (this model is represented by Eq. 2 in the following section).

(2) Effect of impressed I_{corr} on the penetration of rust into the pore structure of concrete at the interface of steel was considered by an empirical coefficient (φ in Eq. 9 in the following section) [13].

(3) The rust was regarded as rigid and its deformation was neglected.

(4) The effect of stirrups on the crack width was neglected in the FE model.

3.2 Model for Corrosion Layer

Considerable researches have been conducted to model the non-uniformity of the corrosion layer around the rebar cross-section. In this paper, the non-uniform corrosion was modeled using a half elliptical model proposed by Yuan and Ji [6] based on the measurement on samples under artificial corrosion environment. Fig. 8 shows the model for the distribution configuration of the corroded rebar cross-section. Furthermore, the growth of the corrosion layer over time can be considered in the model based on the continuous monitor data of steel weight loss using X-ray.

The expression of the model under the polar coordinate is given as follows:

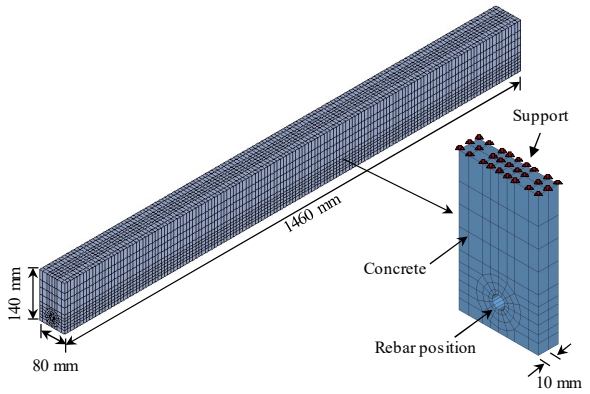

Fig. 7 3D FE model of RC beam using DIANA

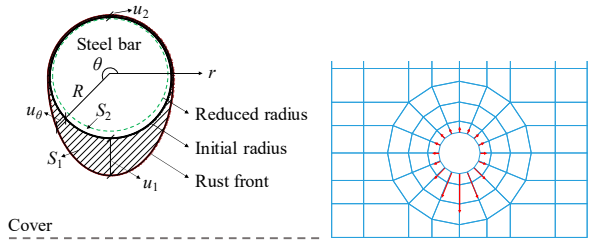

(a) (b)

Fig. 8 (a) Contour line model of rebar of non-uniform corrosion, and (b) Expansion behavior modeled by FE method (Note: the radial displacement is applied on the hole)

$$u_\theta = \begin{cases} u_2 & 0^\circ \le \theta \le 180^\circ \\ \dfrac{(R+u_1)\cdot(R+u_2)}{\sqrt{(R+u_1)\cos^2\theta+(R+u_2)\sin^2\theta}} - R & 180^\circ \le \theta \le 360^\circ \end{cases} \quad (2)$$

where R is the original radius of rabar; u_θ is the corrosion layer thickness in the polar coordinate system; u_1 is the maximum corrosion layer thickness closest to the cover concrete of the beam; u_2 is the corrosion layer thickness at the side far away from the cover concrete; and the shape of the half ellipse is determined by the ratio of u_2/u_1. In this study, u_2/u_1 = 1/30 is assumed according to Du et al. [9].

3.3 Growth of Corrosion Layer

It is well known that not all rust contributes to the build-up of stress and initial cracking of the cover concrete. Some rust may penetrate into the porous zone between the rebar and surrounding concrete. In this paper, the porous zone was assumed to be uniform and its thickness δ was set as 12.5 μm [3]. At this stage, the volume of rust V_{rust1} per element length l can be expressed as:

$$V_{rust1} = V_{poro} + V_{steel1} = 2\pi\delta l + V_{steel1} \quad (3)$$

where V_{poro} is the volume of corrosion products penetrates into the porous zone at the steel/concrete interface; and V_{steel1} is the volume of consumed steel at first stage.

Once the voids in the porous zone are filled completely with rust, tensile stresses initiate in the surrounding concrete. The corrosion status of rebar cross-section is shown in Fig. 8 (a). S_1 denotes the expansion section area of the surrounding concrete, and S_2 is the section area of the corroded part of rebar. The expansion volume V_{exp} per element length l can be written as:

$$V_{exp} = S_1 \cdot l = \frac{1}{2}\pi Rl(u_1 + 3u_2) \quad (4)$$

The volume of rust V_{rust2} per element length l can be expressed as:

$$V_{rust2} = V_{exp} + V_{steel2} \quad (5)$$

where V_{steel2} is the volume of consumed steel at second stage.

The total amount of rust V_{rust} comes from three sources, including the rust that (1) occupies the consumed steel; (2) penetrates into the porous zone at the steel/concrete interface; and (3) induces the expansion pressure and cracking of cover concrete. Therefore, the total volume of rust can be written as:

$$V_{rust} = V_{steel} + V_{poro} + V_{exp} \quad (6)$$

As all rust is produced from the corrosion of rebar, the relationship between V_{rust} and V_{steel} can be written as:

$$V_{rust} = \beta \cdot V_{steel} \quad (7)$$

where β is the magnitude of the ratio of volume expansion of corrosion products, which is taken to be 2.0 [14]; and V_{steel} is the volume of consumed steel.

Substituting Eqs. 3 and 5 into Eq. 7, the total volume of rust can be expressed as:

$$V_{rust} = \frac{4\pi R\delta l + \pi Rl(u_1 + 3u_2)}{2(\beta - 1)} \quad (8)$$

It should be noted that some rust would be deposited into the cracks caused by corrosion. Meanwhile, the amount of rust that penetrates into the surrounding concrete depends on the level of impressed current density [13]. The lower current density may provide an opportunity for rust to fill the pores in the surrounding concrete. In other words, more rust would not contribute to the build-up of stress and induce cracking of surrounding concrete. To simplify the problem, an empirical coefficient φ assumed in 3.1 is determined herein to consider the effect of impressed current density and corrosion level as below:

$$\varphi = a + b \cdot MRw + c \cdot I_{corr}^{d} \quad (9)$$

where φ is the ratio of crack width obtained from FE analysis without considering the effects of the current density and corrosion level to that obtained from experimental results; a, b, c, and d are regression coeffi-

cients; a = 0.9029; b = 10.29; c = 24.15; and d = −0.6626. Eq. 9 is derived based on the experimental results of three beams.

The steel weight loss as the input in the FE model will be modified by an empirical coefficient as follows:

$$Rw' = \varphi^{-1} \cdot Rw \tag{10}$$

where Rw is the steel weight loss at every element length l obtained from experimental data.

Finally, the modified steel weight loss Rw' can be provided by:

$$Rw' = \frac{V_{rust}}{\pi R^2 l} \times 100\% = \frac{4\delta + u_1 + 3u_2}{2(\beta - 1) \cdot R} \times 100\% \tag{11}$$

3.4 Material Model for Concrete

Concrete is modeled with a smeared crack model. The total strain fixed crack model is utilized in the FE analysis. The constitutive model for concrete in tension is shown in Fig. 9. Linear softening curve based on fracture energy is used to model the tensile behavior of concrete. The crack bandwidth h has been set to be equal to the cube root of the volume of the mesh element [12]. The fracture energy G_f was calculated by CEB-FIP Model Code 2010. The area under the tensile stress-strain curve in Fig. 9 is equal to G_f/h. Since the compressive behavior of concrete has little impact on the computational results, concrete is assumed to behave as an ideal elastic material.

4. VERIFICATION AND DISCUSSION

In this paper, an empirical linear model proposed by Vidal et al. [2] was used to predict the crack width distribution as well. The empirical linear expression is as follows:

$$w = K(\Delta A_s - \Delta A_{s0}) \tag{12}$$

where w is the crack width; ΔA_{s0} is the steel cross-section loss necessary for initiating cracks; ΔA_s is the steel cross-section loss in mm^2; and K = 0.0575 according to Vidal et al. [2].

Fig. 10 shows the simulation results of crack width distribution along the beam SP1. It can be seen that the crack width distribution predicted by FE model shows good agreement with the experimental results. Since the higher current density leads to larger crack width and the effect of current density cannot be considered in the empirical model, the distribution of crack width predicted by empirical model is higher than the experimental results at high corrosion levels. Comparing to the results by empirical model, the results of FE model show a relatively continuous distribution of crack width, since the interaction of cover concrete cracking of adjacent cross-sections along the beam can be considered by the 3D FE model.

The area metric $d(F, S)$ proposed by Ferson et al.

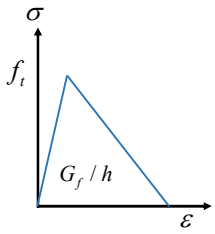

Fig. 9 Linear softening curve of concrete in tension

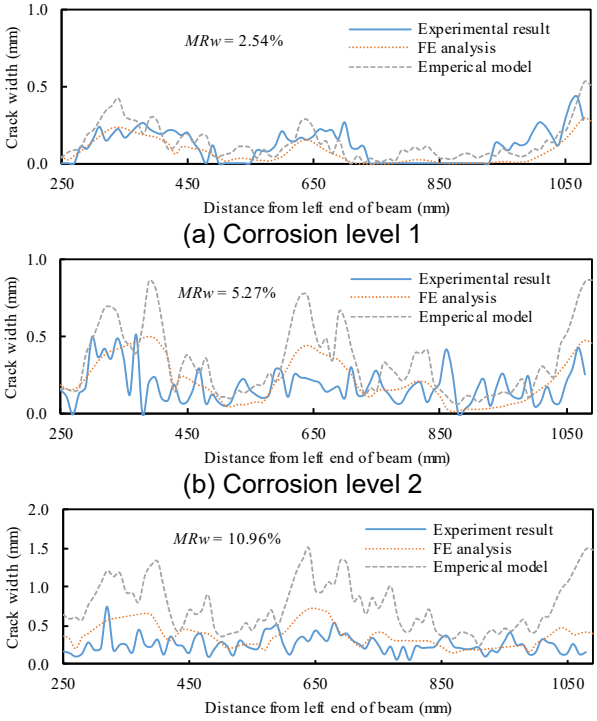

(a) Corrosion level 1

(b) Corrosion level 2

(c) Corrosion level 3

Fig. 10 Predicted and experimental crack width for beam SP1 at different corrosion levels

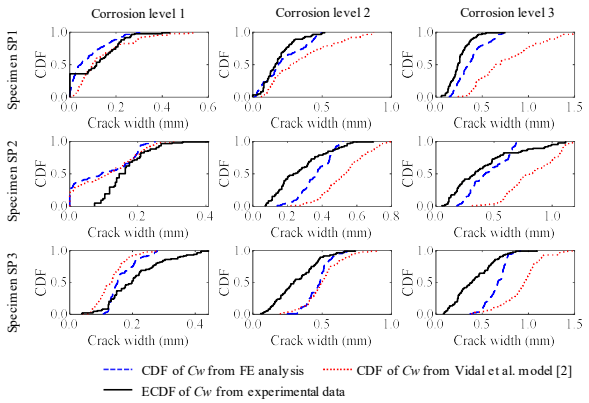

Fig. 11 Area metric for the *Cw* from modeled and experimental results

[15] measures the mismatch between the cumulative distribution functions (CDF) of model output and experimental data and is expressed as:

$$d(F,S) = \int_{-\infty}^{\infty} |F(x) - S(x)| dx \tag{13}$$

where $F(x)$ and $S(x)$ are the CDF predicted by computa-

tional models and the empirical cumulative distribution function (ECDF) of experimental data, respectively. The area metric is used for measuring the disagreement between the CDF of model prediction (FE and empirical) for *Cw* and experimental data. The comparison of CDF of *Cw* between the model-simulated and experimental results is illustrated in Fig. 11. It can be seen that the CDF of *Cw* by FE method is very close to the ECDF of experimental data. However, the CDF of *Cw* by empirical model is far from the ECDF of experimental data. These results indicate that the 3D FE model is capable of predicting the crack width distribution with enough accuracy. The effects of corrosion expansion of adjacent rebar cross-sections can be considered in the 3D FE model. In other words, for an element with a specific *Rw*, the higher the *Rw* of its adjacent elements are, the larger the crack width is. In order to model the corrosion-induced cracking considering the spatial distribution, 3D FE analysis should be performed. The empirical model which links the corrosion level and crack width by a linear equation cannot be used to predict the spatial distribution of crack width.

5. CONCLUSIONS

The non-uniform steel corrosion along the corroded rebar and the associated longitudinal crack width of RC beams at various corrosion levels were monitored by X-ray and digital image processing techniques. A 3D FE model was established to model the distribution of corrosion-induced crack width over the longitudinal RC beams. The following conclusions can be drawn:

(1) The corrosion-induced crack width distributes non-uniformly along the RC beam due to the non-uniform distribution of steel corrosion. The dispersion degree of crack width given steel weight loss increases with the steel weight loss.

(2) The distribution of crack width modeled by the proposed 3D FE model shows a good agreement with the experimental results.

(3) To predict the spatial distribution of crack width, it is necessary to utilize the 3D FE model that can take into account the non-uniform corrosion distribution not only around the rebar perimeter but also along the longitudinal rebar.

REFERENCES

[1] Akiyama, M., Frangopol, D. M., and Yoshida, I. "Time-dependent reliability analysis of existing RC structures in a marine environment using hazard associated with airborne chlorides," Engineering Structures, Vol. 32, No. 11, 2010, pp. 3768–3779.

[2] Vidal, T., Castel, A., and François, R. "Analyzing crack width to predict corrosion in reinforced concrete," Cement and Concrete Research, Vol. 34, No. 1, 2004, pp. 165–174.

[3] Y. Liu., and R. E. Weyers. "Modeling the Time to Corrosion Cracking in Chloride contaminated Reinforced Concrete Structures," ACI Materials Journal, Vol. 95, No. 6, 1998, pp. 675–680.

[4] Chen, J., Zhang, W., and Gu, X. "Modeling time-dependent circumferential non-uniform corrosion of steel bars in concrete considering corrosion-induced cracking effects," Engineering Structures, Vol. 201, 2019, pp. 109766.

[5] Zhao, Y., Yu, J., Hu, B., et al. "Crack shape and rust distribution in corrosion-induced cracking concrete," Corrosion Science, Vol. 55, 2012, pp. 385–393.

[6] Yuan, Y., and Ji, Y. "Modeling corroded section configuration of steel bar in concrete structure," Construction and Building Materials, Vol. 23, No. 6, 2009, pp. 2461–2466.

[7] Lim, S., Akiyama, M., Frangopol, D. M., et al. "Experimental investigation of the spatial variability of the steel weight loss and corrosion cracking of reinforced concrete members: novel X-ray and digital image processing techniques," Structure and Infrastructure Engineering, Vol. 13, No. 1, 2017, pp. 118–34.

[8] Zhang, M., Song, H., Lim, S., et al. "Reliability estimation of corroded RC structures based on spatial variability using experimental evidence, probabilistic analysis and finite element method," Engineering Structures, Vol. 192, 2019, pp. 30–52.

[9] Du, X., Jin, L., and Zhang, R. "Modeling the cracking of cover concrete due to non-uniform corrosion of reinforcement," Corrosion Science, Vol. 89, 2014, pp. 189–202.

[10] Chen, E., and Leung, C. K. Y. "Finite element modeling of concrete cover cracking due to non-uniform steel corrosion," Engineering Fracture Mechanics, Vol. 134, 2015, pp. 61–78.

[11] Zhao, Y. "State-of-art of corrosion-induced cracking of reinforced concrete structures," Journal of Southeast University (Natural Science Edition), Vol. 43, No. 5, 2013, pp. 1122–1134. (in Chinese)

[12] TNO., "DIANA10.3 User's manual, " TNO Building and Construction Research, Delft, 2019.

[13] El Maaddawy, T. A., and Soudki, K. A. "Effectiveness of impressed current technique to simulate corrosion of steel reinforcement in concrete," Journal of materials in civil engineering, Vol. 15, 2003, pp. 41–47.

[14] Molina, F.J., Alonso, C., and Andrade, C. "Cover cracking as a function of rebar corrosion: part 2 – Numberical model," Materials and Structures, Vol. 26, 1993, pp. 532–548.

[15] Ferson, S., Oberkampf, W. L., and Ginzburg, L. "Model validation and predictive capability for the thermal challenge problem," Computer Methods in Applied Mechanics and Engineering, Vol. 197, No. 29–32, 2008, pp. 2408–2430.